

## **Supplementary notes and supplementary figures for paper “A landscape of response to drug combinations in non-small cell lung cancer”**

Nishanth Ulhas Nair<sup>1</sup>, Patricia Greninger<sup>2</sup>, Xiaohu Zhang<sup>6</sup>, Adam A. Friedman<sup>2</sup>, Arnaud Amzallag<sup>2</sup>, Eliane Cortez<sup>2</sup>, Avinash Das Sahu<sup>3</sup>, Joo Sang Lee<sup>4</sup>, Anahita Dastur<sup>2</sup>, Regina K. Egan<sup>2</sup>, Ellen Murchie<sup>2</sup>, Michele Ceribelli<sup>6</sup>, Giovanna S. Crowther<sup>2</sup>, Erin Beck<sup>6</sup>, Joseph McClanaghan<sup>2</sup>, Carleen Klump-Thomas<sup>6</sup>, Jessica L. Boisvert<sup>2</sup>, Leah J. Damon<sup>2</sup>, Kelli M. Wilson<sup>6</sup>, Jeffrey Ho<sup>2</sup>, Angela Tam<sup>2</sup>, Crystal McKnight<sup>6</sup>, Sam Michael<sup>6</sup>, Zina Itkin<sup>6</sup>, Mathew J. Garnett<sup>5</sup>, Jeffrey A. Engelman<sup>2</sup>, Daniel A. Haber<sup>2,6</sup>, Craig J. Thomas<sup>7,8,\*</sup>, Eytan Ruppin<sup>1,\*</sup>, Cyril H. Benes<sup>2,\*</sup>

1 – Cancer Data Science Laboratory, Center for Cancer Research, National Cancer Institute, National Institutes of Health, Bethesda, USA.

2 – Massachusetts General Hospital, Harvard Medical School, Boston, USA.

3 – University of New Mexico, Comprehensive Cancer Center, Albuquerque, New Mexico, USA.

4 – Samsung Medical Center, Sungkyunkwan University School of Medicine, Suwon 16419, Republic of Korea.

5 – Wellcome Trust Sanger Institute, Wellcome Trust Genome Campus, Cambridge, CB10 1SA, UK.

6. Howard Hughes Medical Institute, Bethesda, MD, USA.

7. Division of Preclinical Innovation, National Center for Advancing Translational Sciences, National Institute of Health, Rockville MD 20850, USA.

8. Lymphoid Malignancies Branch, Center for Cancer Research, National Cancer Institute, National Institutes of Health, Bethesda, MD 20892, USA.

\* –These authors jointly supervised this work. Cyril H. Benes – [cyrilbenes@gmail.com](mailto:cyrilbenes@gmail.com); Eytan Ruppin – [eytan.ruppin@nih.gov](mailto:eytan.ruppin@nih.gov); Craig J. Thomas – [craigt@mail.nih.gov](mailto:craigt@mail.nih.gov)

## Supplementary Notes

### 1. Synergy computation

Synergy scores are computed using the Bliss model<sup>1</sup>. The lower the score, the more synergistic the drug-combination is. A drug combination is synergistic if its score is less than 1.

We defined a drug pair to be synergistic in the following manner: In each cell line and combination (for a particular library drug dose), we have cell counts measurements (day 6) upon library+anchor (LA) combination, library-only treatment (L), anchor-only treatment (A) and with only DMSO control treatment (C). Synergy score =  $(LA/A) / (L/C)$ .

Consider the following example to calculate synergy shown in Supplementary Table 1:

**Supplementary Table 1:** Example to calculate synergy shown.

Cell Line	Anchor ID	Library ID	Cell Count (from drugged plates data)
X	DMSO	DMSO	500
X	DMSO	L	450
X	A	DMSO	400
X	A	L	150

Library drug alone response Plate (I) compared to DMSO control =  $450 / 500$

Library + Anchor Plate (II) Compared to Anchor alone =  $150 / 400$

Synergy (delta from bliss) =  $(\text{Library + Anchor Plate (II) Compared to Anchor alone}) / \text{Library drug alone response Plate (I) compared to DMSO control} = (150/400) / (450/500)$

We calculate synergy for each cell line and for every drug pair in each cell line for all doses D1 to D5 (for library drugs). We then compute the median value of the 2 replicates to get a synergy value for each drug pair for each cell line for a particular library dose.

## 2. Coverage analysis

We ask the question: for a given anchor, what is the minimum number of library drugs required so that at least 80% of the cell lines have one high synergy?

To address the above question, we consider the 21x242 drug combos across 81 cell lines. High synergy was defined based on second-best synergy (top 5% threshold). For each anchor, we have a binary matrix for all cell lines and libraries – a matrix of 1s and 0s, where 1 stands for high synergy and 0 otherwise. We used a simple greedy algorithm to compute the minimum no. of library drugs so that at least 80% of the cell lines have one high synergy. Since it is a greedy algorithm, it is an approximate solution.

The greedy algorithm used is similar to the classic greedy algorithm for the set covering problem<sup>2-4</sup>.

-

Our greedy algorithm is as follows:

- a) For a given anchor, we have a binary matrix (say M) for all cell lines and libraries – a matrix of 1s and 0s, where 1 stands for high synergy and 0 otherwise. Let D be the counter for the no. of drugs considered. Set D=0. Also set the cell lines considered as PC = NULL SET.
- b) We pick the library drug with the maximum high synergy cell lines for the given anchor in matrix M. Set  $D = D + 1$ .
- c) We remove those high synergy cell lines from M (let C be the names of those cell lines). So, we get a new smaller matrix for M. Calculate  $PC = \text{union}(PC, C)$ .
- d) Check if  $(\text{length\_of\_PC} / \text{total\_no\_of\_cell\_lines}) * 100 < 80\%$ . If so, repeat from step b.

We repeated the above analysis for different percentages of cell lines (from 50% to 100%).

### **3. Potential mechanisms underlying some notable synergistic combinations**

The first involves the NMPRT/NAMPT inhibitor daporinab (FK866), which was seen to yield HSA and synergies across many cell lines in combination with olaparib. PARP enzymes are thought to consume a large amount of cellular NAD as their substrate for PARylation on targets. Daporinab, by inhibiting NAMPT, lowers the levels of NAD in cells and this change in substrate availability has been previously suggested to underlie the synergy between PARP and NAMPT inhibitors<sup>5</sup> with potential impact for the treatment of Ewing's sarcoma<sup>6</sup>.

Second, a number of synergies were observed with the insulin/insulin growth factor receptors inhibitor BMS754807. This outcome most likely corresponds to the well described feedback inhibition on IRS1 (Insulin Receptor Substrate 1), a key adaptor in the Insulin Receptor pathway that is subject to inhibitory phosphorylation in an mTORC1 dependent manner and was recently described to imply degradation of IRS1 following phosphorylation by mTORC1 itself<sup>7,8</sup>. BMS754807 synergizes less with BYL719 or GDC0941 than with OSI-027 even though mTORC1 is under the control of PI3K via AKT phosphorylation of TSC (Manning & Cantley, 2007). This is possibly due to the presence of other compensatory feedback loops that are not modulating the viability outcome when mTORC1 itself is targeted. In contrast to the PI3K inhibitors alpelisib (BYL719, PI3K $\alpha$ ) and pictilisib (GDC0941, pan PI3K), the MTORC inhibitor OSI027 synergizes broadly with the farnesyl transferase inhibitor tipifarnib (Figure 3G, Figures 6-7). This is an unexpected outcome that seems to indicate either unappreciated activity of farnesyl transferase linked to mTORC1/2, perhaps linking HRAS to mTORC or an unsuspected off target of one of the two inhibitors. Interestingly, a recent study identified MTORC2 as a direct binding partner of RAS proteins albeit not specific to HRAS over other RAS isoforms<sup>9</sup>.

Thirdly, targeting the RB pathway has been a long-standing interest in cancer therapeutics<sup>10</sup>. Inhibition of CDK4/6, which regulates cell cycle entry via the control of RB1/E2F complex, has in recent years been employed in multiple clinical settings. Single agent activity has been observed

in preclinical models across different cancer types and promising results obtained in non-small-cell lung cancer (NSCLC) models<sup>11</sup>. In addition to improving the outcome of hormonal therapy in ER positive breast cancer inhibitors<sup>12</sup> of CDK4/6 are considered candidate combination agents in several cancers<sup>13</sup>. CDK4 depletion in a mouse model of NSCLC driven by KRAS induces senescence and tumor regression<sup>14</sup> and single agent activity of abemaciclib (LY2835219) a potent CDK4/6 inhibitor was seen in KRAS driven NSCLC human tumors<sup>15</sup>. However, further exploration of this paradigm has not led to improvement in overall survival of patients in the single agent setting<sup>16</sup>. More recently, a preclinical study reported activity of CDK4/6 targeting in NSCLC with loss of SMARCA4 (a component of the SWI/SNF chromatin regulator complex)<sup>17</sup>. There is thus considerable interest in building combinatorial strategies around CDK4/6 inhibition, in particular for KRAS mutant NSCLC. Here we identify mTOR and MEK inhibitors as best combination partners for palbociclib (Supplementary Figure 3). However, overall, our results in vitro and with limited time of exposure to drugs, show a modest number of synergies with high sparsity across cell lines. Nevertheless, longer time of treatment or non-cell autonomous effects could make these combinations beneficial in patients. Several clinical trials are poised to test the efficacy of MAPK pathway inhibitors in combination with CDK4/6 inhibition in NSCLC (for example, NCT03170206 for MAPK and NCT03065062 for mTOR/PI3K) and future combinations would be critical to address emerging resistance mechanisms<sup>18</sup>. In addition, different CDK4/6 inhibitors vary in their target selectivity such that across the three approved CDK4/6 inhibitors, specific combinations might display differential synergies and/or clinical benefit<sup>19</sup>.

Our fourth set of interesting combinations involves SRC kinases. These enzymes, including p60c-Src and the closely related Src Family Kinases (SFK) members FYN and YES, are a group of non-receptor tyrosine kinases that have long been implicated in several hallmarks of cancer<sup>20</sup>. In particular, SFKs regulate adhesion and motility mediated by integrins in coordination with the tyrosine kinase FAK as well as growth factor signaling. SFK are for example known to play a role in the activation of the MEK-ERK/MAPK pathway in several contexts and recent mechanistic studies support a model whereby SFKs can coordinate various signaling inputs with growth factor sensing by RTKs<sup>21</sup>. Their targeting in tumors has long been elusive however and somewhat surprisingly, no mutations are found in these kinases in tumors. The multi-targeted kinase inhibitor dasatinib is a potent inhibitor of Bcr-Abl and was approved for use in Philadelphia positive chronic

myelogenous leukemia (CML) and Acute Lymphoblastic Leukemia (Ph+ ALL) in 2006<sup>22</sup>. It also potently inhibits SRC and other SFKs and was used here to probe the potential of an approved drug targeting SFKs to yield beneficial combinations in NSCLC. We found that TAE-684 synergizes broadly with dasatinib (Supplementary Figure 3,5). This is surprising since the kinase inhibitor TAE-684 was designed to inhibit the ALK tyrosine kinase which is an oncogene in NSCLC when fused to EML4<sup>23</sup>. ALK is not normally expressed in NSCLC and ALK inhibitors are thus not broadly expected to be active outside of the ALK fusion driver context. This synergistic interaction between dasatinib and TAE-684 is thus most likely due to targeting of other kinase(s) than ALK, possibly IGF1R<sup>24</sup>. Two Insulin Receptor (IR) / Insulin Growth Factor 1 Receptor (IGF1R) inhibitors were used. Intriguingly, only one, BMS-754807 but not linsitinib displayed a very high number of synergies with dasatinib and indeed was the top synergizing drug with dasatinib. This strongly suggests that the synergies seen with the BMS compound are either not due to IR/IGF1R targeting or that additional targeting is needed to yield synergy (Supplementary Figure 4,5). This illustrates again the challenge brought by polypharmacology when trying to assign mechanisms to the observed synergies as well as how polypharmacology can result in differential synergistic outcome across compounds that are as single agents yielding similar activity profiles.

Fifth, a number of strong synergies were seen with the pan Aurora Kinase (AURK) inhibitor tozasertib (VX-680, used as an anchor) (Figure 3G, 4D, Supplementary Figures 7-8). Three additional AURK inhibitors were used in the drug library: Barasertib (AZD-1152) which is selective for Aurora Kinase B over Aurora Kinase A, alisertib (MLN8237) and ENMD-981693 which are selective for Aurora kinase A. Synergistic activity was detected between AURK inhibitors and HDAC inhibitors (Supplementary Figure 7) in line with previous reporting<sup>25</sup>. Interestingly, while both AURK and Cyclin Dependent Kinases are involved in cell cycle progression CDK inhibitors did not display the same broad pattern of synergies as AURK inhibitors (Supplementary Figure 7). Thus, cell cycle inhibition does not appear to be sufficient to explain the AURK inhibitors results and perhaps a more specific outcome of inhibiting mitotic progression with AURK inhibitors is at play or other non-mitotic targets<sup>26-28</sup> of AURK are involved. Across anchors, different AURK inhibitors display differential synergy profiles. For example, while both barasertib and alisertib synergize with the BCL2 family targeting compound

navitoclax, ENMD-981693 shows more synergies across cell lines with the CHK inhibitor AZD7762 than other AURK inhibitors. In contrast, all 4 AURK inhibitors tested synergize with the HDAC inhibitor vorinostat across many cell lines, albeit with only partial overlap of cell lines presenting synergy (Supplementary Figure 7). Thus, inhibition of either AURKA, AURKB (and AURKC) appears to have distinct outcomes in the combination setting. The mechanistic underlying of this observation is unclear but could be either a specific, possibly non-mitotic function of AURKs, a specific state of cell cycle arrest obtained with one inhibitor versus another, or alternate targets engaged by different inhibitors. Nevertheless, here and in other combination screens<sup>29</sup> targeting AURK in combination with different growth factors, survival and DNA damaging agents could yield relatively frequent synergistic outcomes. Interestingly, AURKA has been linked to PI3K inhibition response in breast cancer and to resistance to EGFR inhibition in NSCLC<sup>30,31</sup>.

Sixth, the BCL2 family inhibitor synergizes with many drugs in the present study in keeping with previous results obtained in our studies on melanoma cell lines where navitoclax was characterized as a broad sensitizer to many other drugs<sup>32</sup>. This makes intuitive sense for a pro-apoptotic agent. In particular, some but not all inhibitors of the cell cycle present with numerous synergies when combined with navitoclax. For example, dinaciclib an inhibitor of multiple CDKs, BI-2536 and GW843682X inhibitors of Polo Like Kinases (PLK), or AT9283, alisertib and barasertib, inhibitors of AURKs are some of the drugs with the most synergies. There is precedent for the combination of dinaciclib and ABT263 to synergize via downregulation of MCL1, a major resistance factor to navitoclax as mentioned in the results section. Somewhat less expected are synergies observed between the ETC complex V inhibitor oligomycin and navitoclax, although a recent report on CLL identified oxidative phosphorylation as a regulator of BCL2 inhibitor sensitivity and demonstrated synergy between oligomycin and BCL2 targeting in lymphoid cells<sup>33</sup>. BCL2 family members are not only involved in apoptosis by regulating the release of cytochrome C from the mitochondria but also in the maintenance of mitochondrial network function through regulation of fission-fusion cycle and possibly other means<sup>34</sup>. Thus, the observed synergies between complex V inhibition and BCL2 inhibition could represent impact on mitochondrial integrity or sensitization to mitochondrial release of cytochrome C.

Seventh, the mitochondrial ATPsynthase inhibitor oligomycin was ranked 6th when considering median HSA score across cell lines for trametinib. This represented strong but relatively uncommon synergies and thus was also not flagged in the impact score analysis. Notably, oligomycin was the only drug with no obvious signaling network connection to MEK in the top 12 drugs ranked by median HSA. Oligomycin was also synergistic with OSI-27, pictilisib, dasatinib, navitoclax and perhaps less surprisingly with phenformin. These results suggest that disruption of ETC, while not necessarily lethal on its own, is creating vulnerability to core growth factor signaling inhibition by PI3K or ERK pathway inhibition.

#### **4. Self-addition breaking and limitation of statistical independence modeling**

A simple explanation for self-additive coherence breaking is as follows: Consider a scenario where doubling the dose of a drug yields a doubling of the viability effect. Then consider what happens if the outcome of dose A for this drug is 80% viability. Doubling the dose (adding the same treatment to itself,  $A \times 2$ ), based on statistical independence would be expected to yield 64% viability ( $0.8 \times 0.8$ ). Thus, in this case yielding a synergy score of 0.625 ( $0.08/0.64$ ). Now consider the same drug but with an initial dose yielding 40% viability. In this case the expected outcome is 16% ( $0.4 \times 0.4$ ; or 40% of 40%) and the observed outcome is 20%, meaning that no synergy is detected. Now, consider a drug that has a shallower dose response curve with a doubling of the dose yielding a 1.2-fold change in viability. This time, starting at 80% for dose A the expected outcome of 64% for  $(A) \times 2$  is compared to an observed outcome of 0.67 ( $0.8/1.2$ ) which does not represent synergy based on statistical independence (67% compared to 64%). Thus, both steepness of the curve and dosing (where on the dose response curve the data is acquired) impact the synergy call outcome. Importantly, analysis of single agent data in the present screen reveals that dosing yielded a broad range of viability values (Supplementary Figure 1) and that viability ratio for two consecutive doses chosen experimentally to be  $\sqrt{10}$  apart (every other dose matches a 10-fold dilution) has a median value of 1.04 (1.14 for the top 25% ratio values). By contrast, the HDAC inhibitor vorinostat that shows self-additive synergy has a median ratio of viability across two consecutive doses of 1.44 (2.11 for the top 25% ratio values).



## 5. Comparison of *in vitro* and *in vivo* NSCLC models

Gao et al. (2015)<sup>35</sup> tested 5 drug combinations across 36 NSCLC mouse PDX models. While none of these drug combinations were exactly the same as what we used in our *in vitro* original drug combination screens, 3 drug combinations had similar drug targets. These three drug combinations in the Gao paper are: BKM120 (panPI3K inhibitor) and binimetinib (MEK inhibitor); BYL719 (PI3Kalpha inhibitor) and LGH447 (PIM inhibitor); LFW527 (IGF1R inhibitor) and binimetinib (MEK inhibitor).

Since, there is no clear concept of synergy in this mouse models dataset, in the Gao et al paper<sup>35</sup>, we checked the percentage of PDX models in which drug combinations are more effective than both individual drugs (based on the percent tumor volume change after treatment; one-sided Wilcoxon rank-sum test,  $P < 0.05$ ). We compared it with the percentage of highly synergistic cell lines in the correspondingly mapped drug combinations in our original *in vitro* screen (top 5 percentile chosen as the threshold of high synergy). The results are summarized in Supplementary Table 2. As seen, we see a very good concordance between our drug combination *in vitro* screen and in the PDX models based on the fraction of highly synergistic/effective models for PI3K and MEK inhibitors, PI3K and PIM inhibitors, IGF1R and MEK inhibitors.

**Supplementary Table 2:** Comparing drug combinations between *in vitro* and *in vivo* NSCLC models.

<b>Drug targets</b>	<b>PDX screen drug combination (percentage of NSCLC PDX models in which the combinations is more effective than both individual drugs is shown).</b>	<b>Original <i>in vitro</i> screen drug combination for the mapped drugs based on similar targets (percentage of highly synergistic cell lines shown)</b>
<u>PI3K &amp; MEK inhibitor combination</u>	BKM120 & Binimetinib = <b>20.69%</b> (6 out of 29 models)	Alpelisib & Trametinib = 24.32%  Alpelisib & Selumetinib = 16.22%  Pictilisib & Trametinib = 31.58%  Pictilisib & Selumetinib = 22.37%  Mean value of high synergies of these combinations = <b>23.62%</b>
<u>PI3K &amp; PIM inhibitor combination</u>	BYL719 & LGH447 = <b>10.34%</b> (3 out of 29 models)	Alpelisib & AZD1208 = 8.11%  Alpelisib & SGI-1776 = 4.05%  Pictilisib & AZD1208 = 17.11%  Pictilisib & SGI-1776 = 3.95%  Mean value of high synergies of these combinations = <b>8.31%</b>
<u>IGF1R &amp; MEK inhibitor combination</u>	LFW527 & Binimetinib = <b>12%</b> (3 out of 25 models).	Linsitinib & Trametinib = 10.96%  Linsitinib & Selumetinib = 9.59%  Mean value of high synergies of these combinations = <b>10.28%</b>

**Supplementary Table 3: Cell lines used in this study.**

ID	Cell Line	Source	CatalogNumber
850	201T	UPMC	NA
752	A-427	ATCC	HTB-53
677	A549	ATCC	CCL-185
888	ABC-1	JHSF	JCRB0815
756	BEN	DSMZ	ACC 254
851	CAL-12T	DSMZ	ACC 443
679	ChaGo-K-1	ATCC	HTB-168
864	COR-L 105	ECACC	92031918
865	COR-L23	ECACC	92031919
886	EBC-1	JHSF	JCRB0820
854	EPLC-272H	DSMZ	ACC 383
890	H3255	NCI	NA
872	HARA	JHSF	JCRB1080.0
855	HCC-15	DSMZ	ACC 496
856	HCC-366	DSMZ	ACC 492
857	HCC-44	DSMZ	ACC 534
858	HCC-78	DSMZ	ACC 563
859	HCC-827	DSMZ	ACC 566
860	LCLC-103H	DSMZ	ACC 384
861	LCLC-97TM 1	DSMZ	ACC 388
871	LK-2	JHSF	JCRB0829
862	LOU-NH91	DSMZ	ACC 393
879	LU99A	JHSF	JCRB0044
801	NCI-H1299	ATCC	CRL-5803
1243	NCI-H1395	ATCC	CRL-5868
812	NCI-H1437	ATCC	CRL-5872
813	NCI-H1563	ATCC	CRL-5875
815	NCI-H1623	ATCC	CRL-5881
1245	NCI-H1648	ATCC	CRL-5882
791	NCI-H1650	ATCC	CRL-5883
816	NCI-H1651	ATCC	CRL-5884
792	NCI-H1666	ATCC	CRL-5885
818	NCI-H1703	ATCC	CRL-5889
819	NCI-H1734	ATCC	CRL-5891
820	NCI-H1755	ATCC	CRL-5892
794	NCI-H1792	ATCC	CRL-5895
821	NCI-H1793	ATCC	CRL-5896
823	NCI-H1915	ATCC	CRL-5904
824	NCI-H1944	ATCC	CRL-5907
755	NCI-H1975	ATCC	CRL-5908
1136	NCI-H1993	ATCC	CRL-5909
796	NCI-H2009	ATCC	CRL-5911
825	NCI-H2023	ATCC	CRL-5912
827	NCI-H2085	ATCC	CRL-5921
847	NCI-H2087	ATCC	CRL-5922
841	NCI-H2170	ATCC	CRL-5928
832	NCI-H2228	ATCC	CRL-5935
800	NCI-H23	ATCC	CRL-5800
833	NCI-H2342	ATCC	CRL-5941
834	NCI-H2347	ATCC	CRL-5942
835	NCI-H2405	ATCC	CRL-5944
1180	NCI-H3122	DFCI	NA
802	NCI-H358	ATCC	CRL-5807
840	NCI-H441	ATCC	HTB-174
753	NCI-H460	ATCC	HTB-177
842	NCI-H520	ATCC	HTB-182
803	NCI-H522	ATCC	CRL-5810
797	NCI-H596	ATCC	HTB-178
806	NCI-H647	ATCC	CRL-5834
807	NCI-H650	ATCC	CRL-5835
799	NCI-H661	ATCC	HTB-183
680	NCI-H727	ATCC	CRL-5815
808	NCI-H838	ATCC	CRL-5844
868	PC-14	ECACC	90071810
877	PC-3 [JPC-3]	JHSF	JCRB0077
870	RERF-LC-KJ	JHSF	JCRB0137
848	SK-LU-1	ECACC	93120835
843	SK-MES-1	ATCC	HTB-58
844	SW 673	ATCC	CRL-2170
839	SW900	ATCC	HTB-59
678	UMC-11	ATCC	CRL-5975
8018	Calu-6	ATCC	HTB-56
8040	EKVX	NCI	NA
8072	HOP-62	NCI	NA
8075	IA-LM	RIKEN	RCB0554
8103	LC-2-ad	RIKEN	RCB0440
8111	LXF-289	DSMZ	ACC265
8130	NCI-H1355	ATCC	CRL-5865
8132	NCI-H2126	ATCC	CCL-256
8133	NCI-H322M	NCI	NA
8232	EMC-BAC-2	WTSI	NA

**Supplementary Data**

Supplementary data S1-S11 are provided separately in Excel files. Supplementary data S12 is a compressed (zip) folder.

## Supplementary Figures

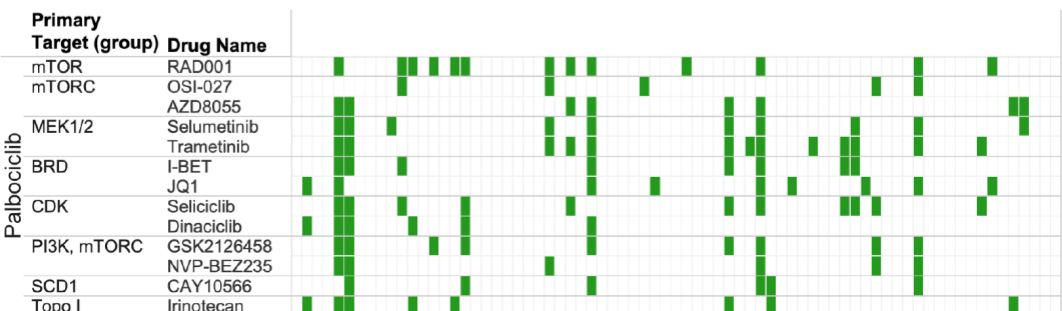
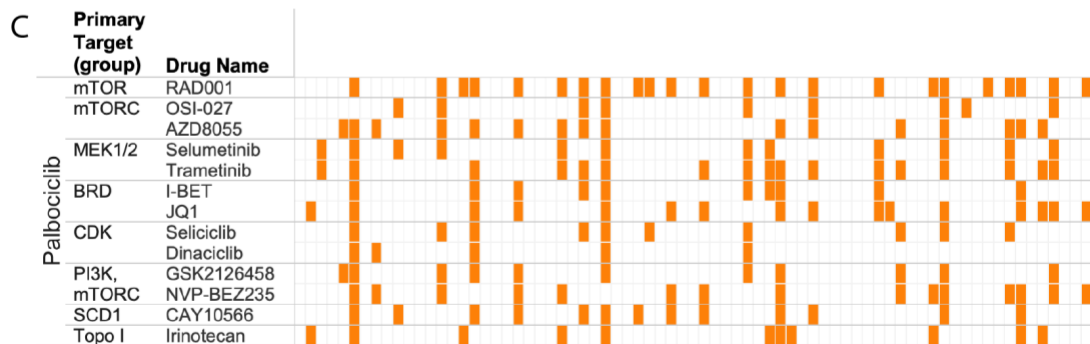


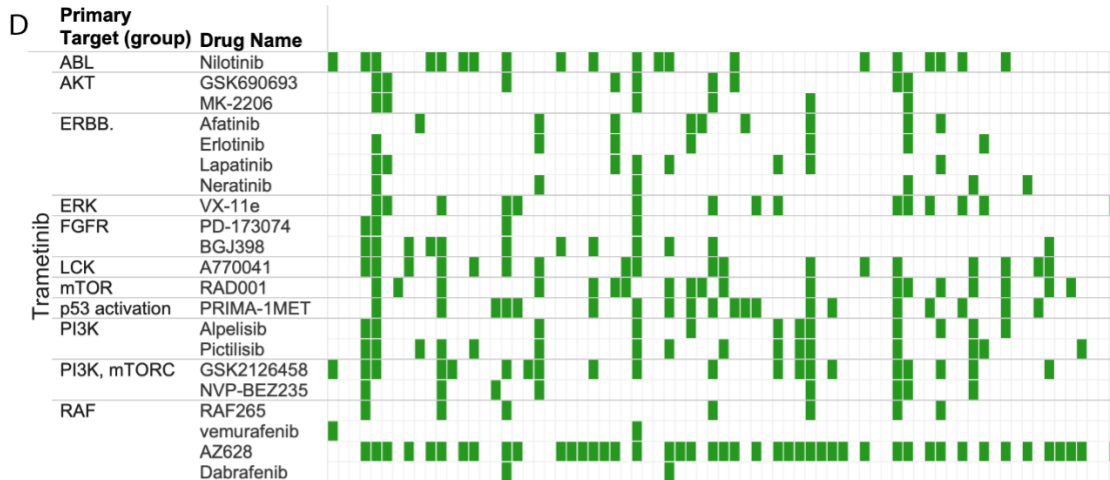
**Supplementary Figure 1: Overview of the dataset and response to single agents.** A: Coverage of the cell line collection. The 81 cell lines (rows) are shown with key cancer genes altered to the right of the heatmap displaying data acquired and passing quality control. The number of biological replicates (Bio Replicates) corresponding to independent days of cell seeding are indicated by the color scheme indicated at the top right. B. Viability response to anchor drugs, the distribution of viability values (across all 81 cell lines) is represented. C. Viability response to library drugs: For each library drugs the range of viability obtained with the indicated drug across the 81 cell line collection is plotted. All 5 doses are plotted together for each drug to demonstrate the overall range of viability obtained. The box plots have median center, 25 and 75 percentiles (Q1 and Q3) as bounds of the box, the minima and maxima being  $Q1 - 1.5 \times IQR$  and  $Q3 + 1.5 \times IQR$  (with IQR being interquartile range).



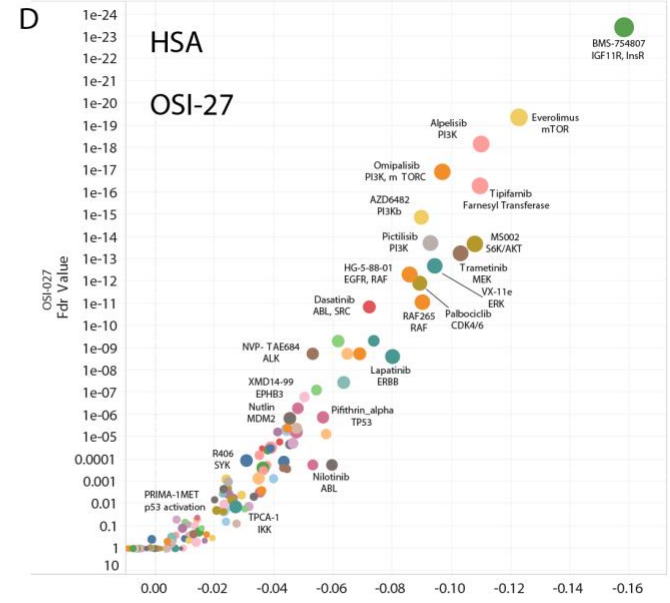
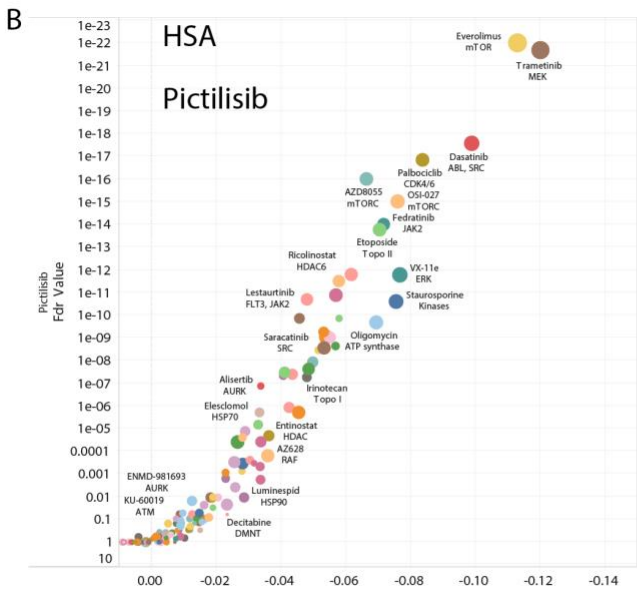
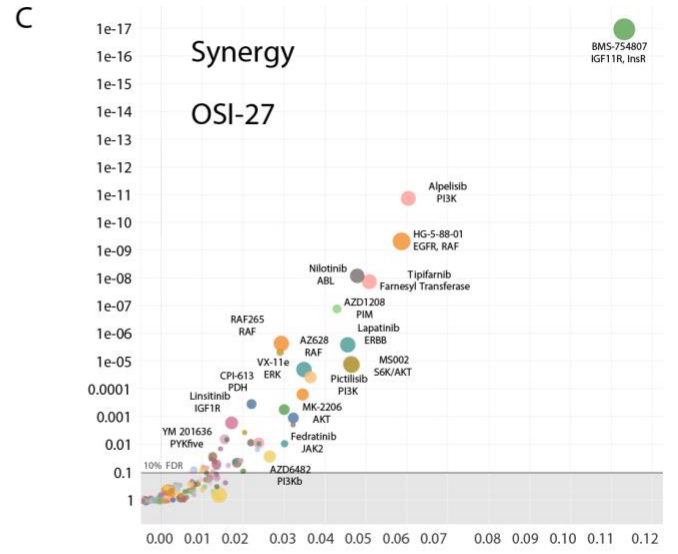
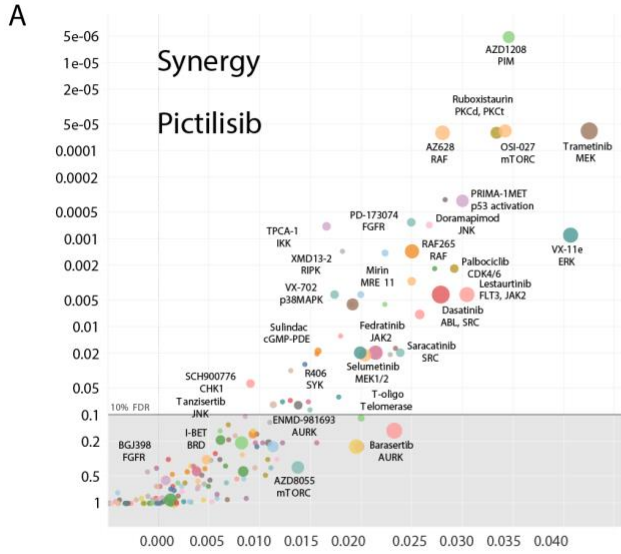


**Supplementary Figure 2: Profile of synergy counts across all tested combinations.** For each combination between the indicated library drug (row) and anchor drug (column) the number of cell lines harboring synergy is depicted by a bar. The size of the bar is proportional to the number of cell lines harboring synergy with maximum size set at 53 (maximum number of cell lines presenting with synergy). Synergy count is based on a synergy score threshold of 0.8.

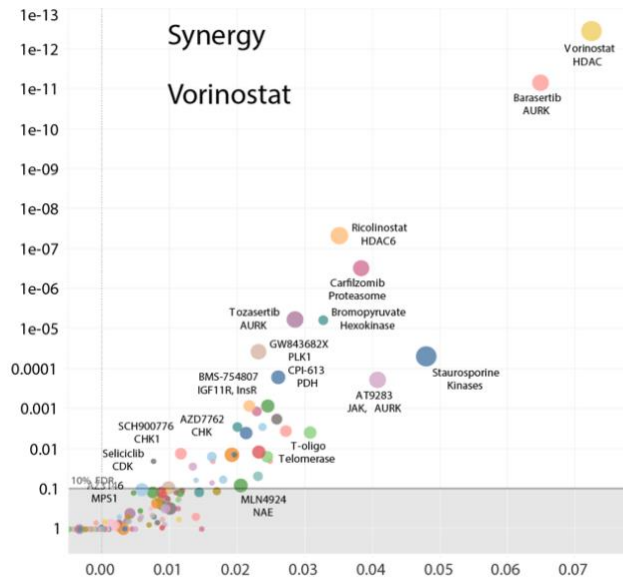




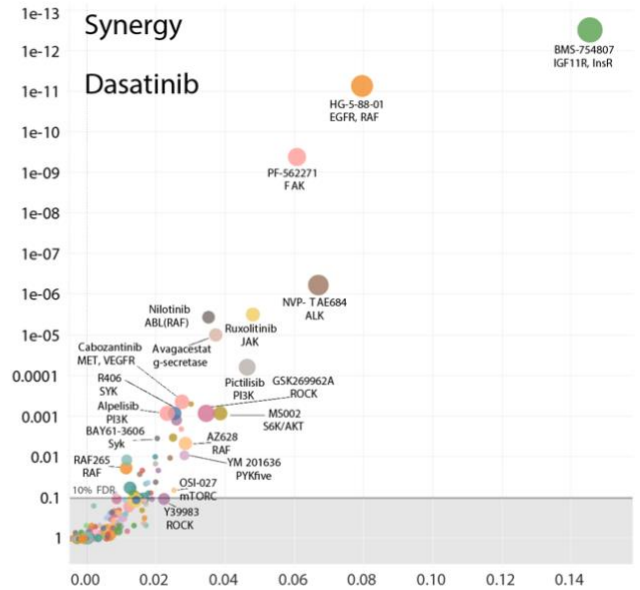
**Supplementary Figure 3: Pattern of synergies and HSA events across related drugs.** Several examples of patterns obtained for drugs with related targets are shown for some of the anchors. A-E: Cell lines (columns) are in the same order across rows to allow for pattern comparison. Cell lines harboring HSA (orange) or synergy (green) are colored accordingly. The same thresholds for synergy and HSA are used across all panels. Anchors for the different panels are: A, Alpelisib (PI3Kalpha); B, Pictilisib (pan PI3K); C, Palbociclib (CDK4/6); D, Trametinib (MEK1/2); E, Dasatinib (ABL, SRC).



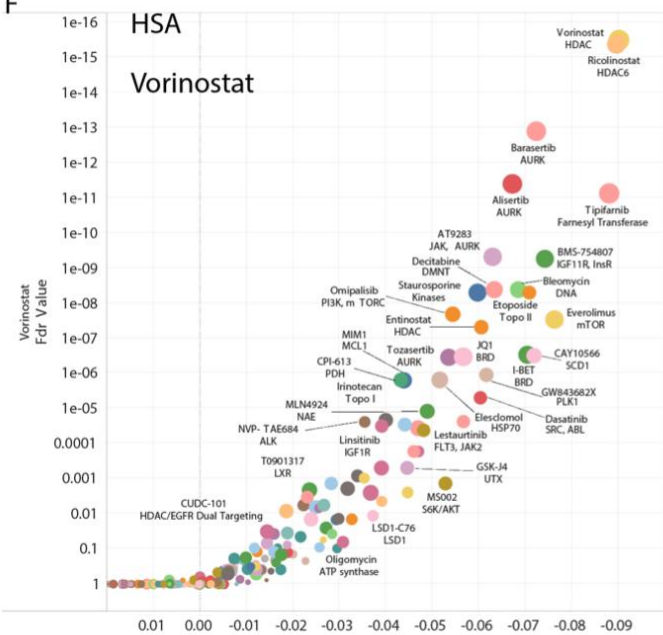
E



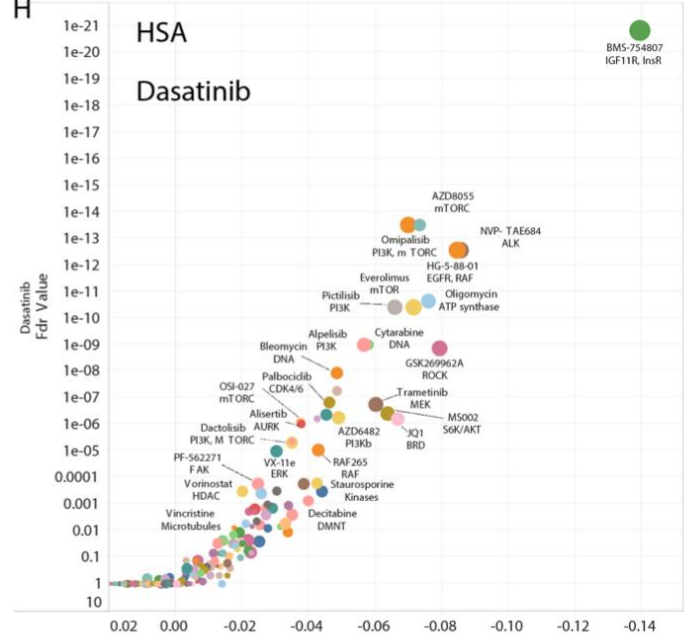
G



F



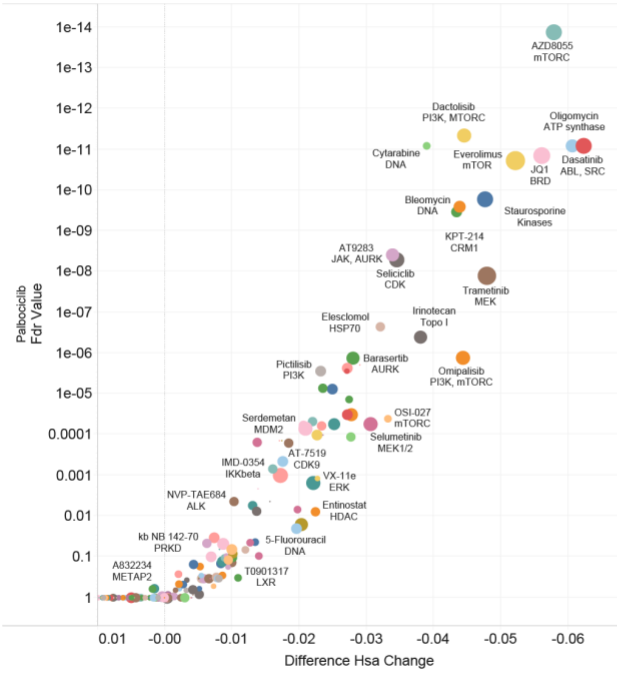
H



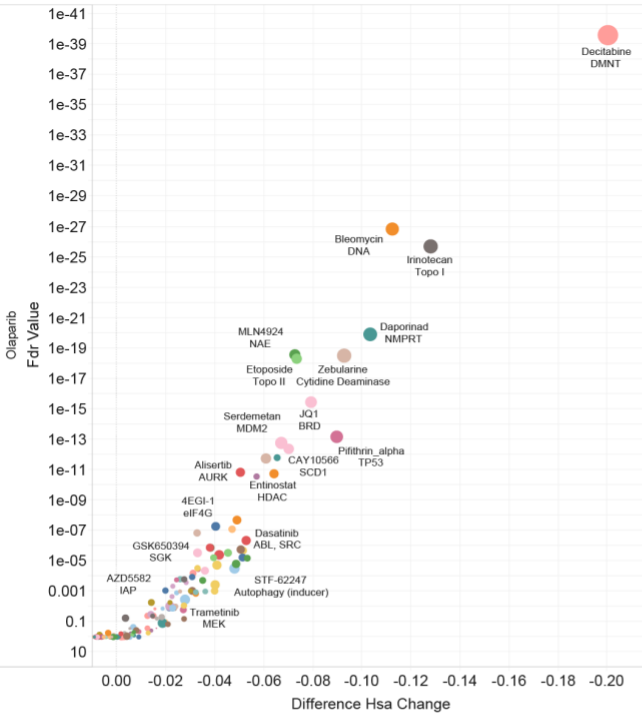
**Supplementary Figure 4: Distribution of synergy and HSA scores for selected anchors illustrates global consistency of the two scoring metrics.** The impact score for each combination is plotted. X axis: Differential median synergy score across cell lines corresponding to the Log10 ratio of the median synergy (or HSA) score for the indicated library drug over median score of all

other drugs. Y axis: FDR value for statistical enrichment of synergies for the plotted combination over all other tested combinations (with the same anchor). The size of the dots represents the percentile of synergy scores for a given combination falling within the top 5% of all synergy scores for the whole screen (all anchors). Anchors: Pictilisib (pan PI3K), OSI-27 (mTORC), Votinostat (HDAC), Dasatinib (ABL, SRC).

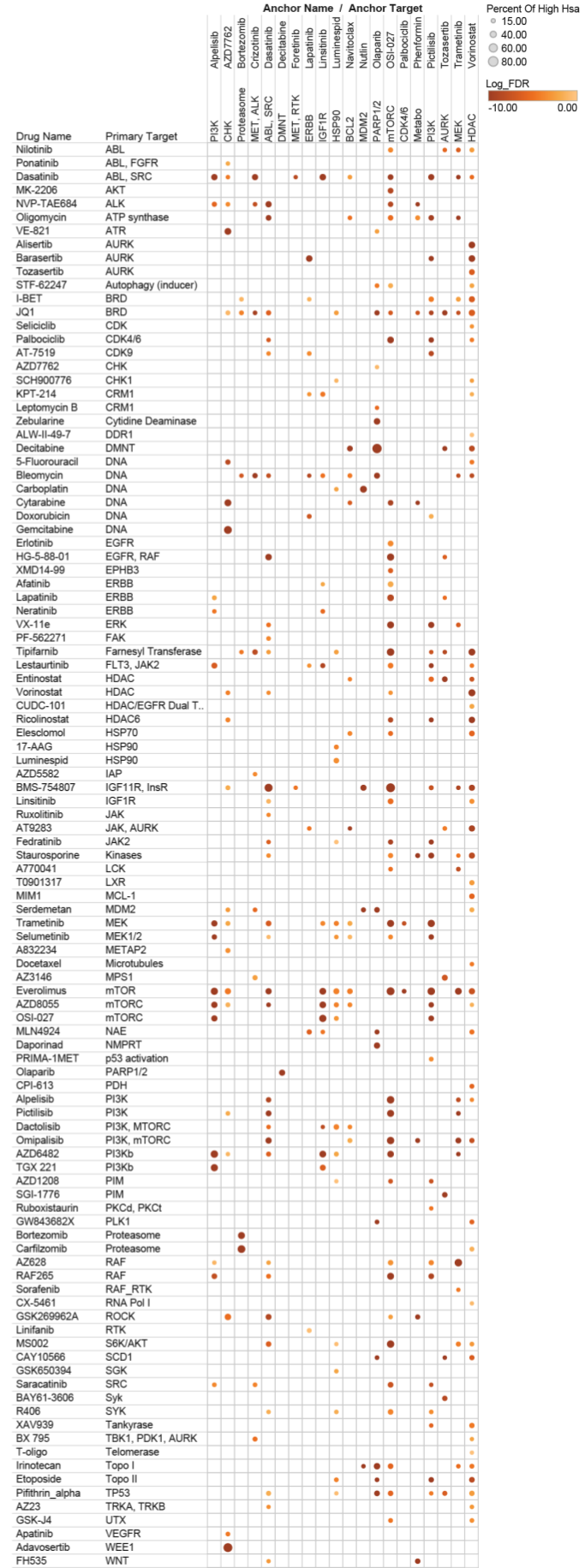
A



B



C

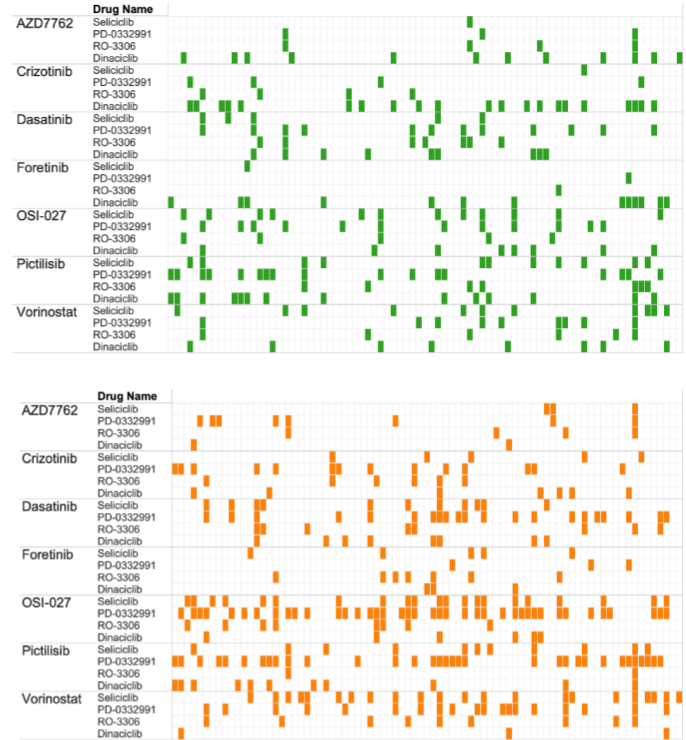
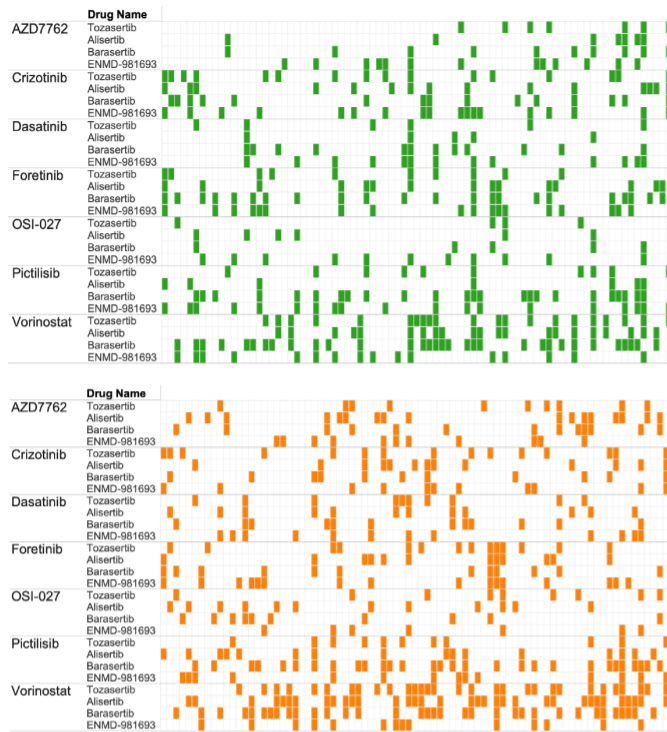




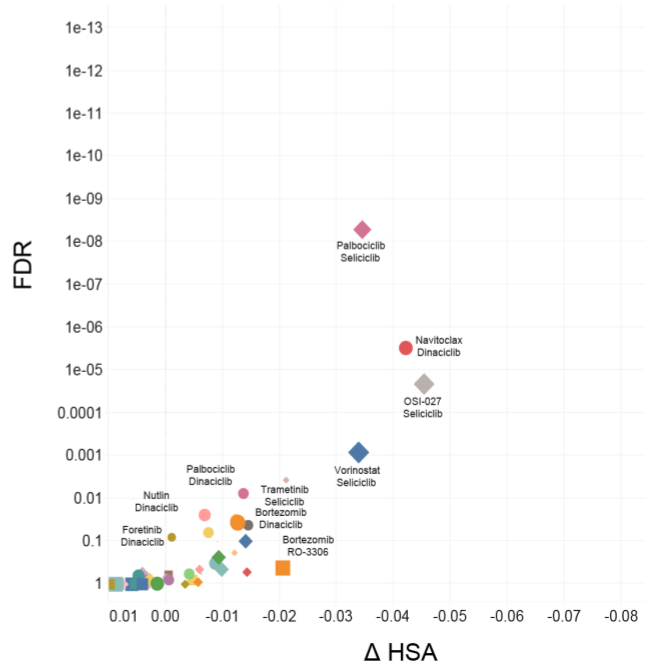
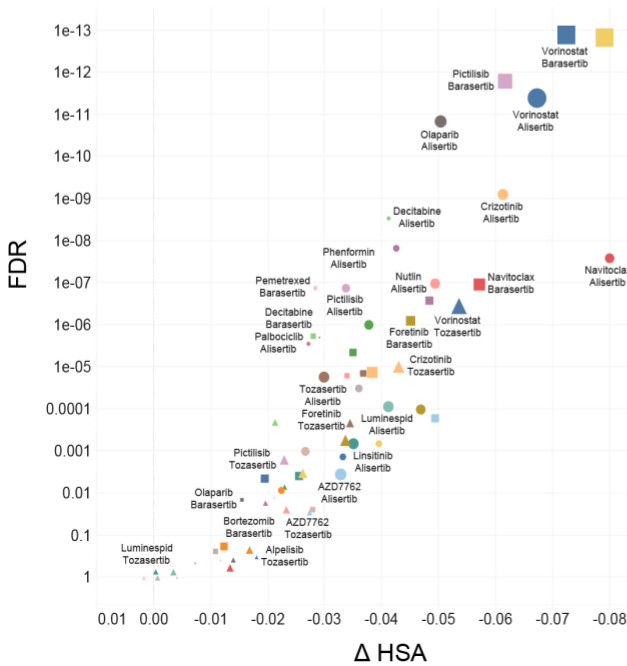
**Supplementary Figure 5: HSA Scores for selected drugs and overall HSA score matrix.** A and B, HSA impact scores for the anchors palbociclib (CDK4/6) and Olaparib (PARP). C: Overview of HSA scores across tested combination. Combinations yielding HSA in at least 15% of the cell lines tested are shown. The size of the dot corresponds to the percentile of cell lines with HSA and the shade to the statistical enrichment of HSA events for the indicated combination over all other tested combinations (darker corresponds to lower FDR).



A

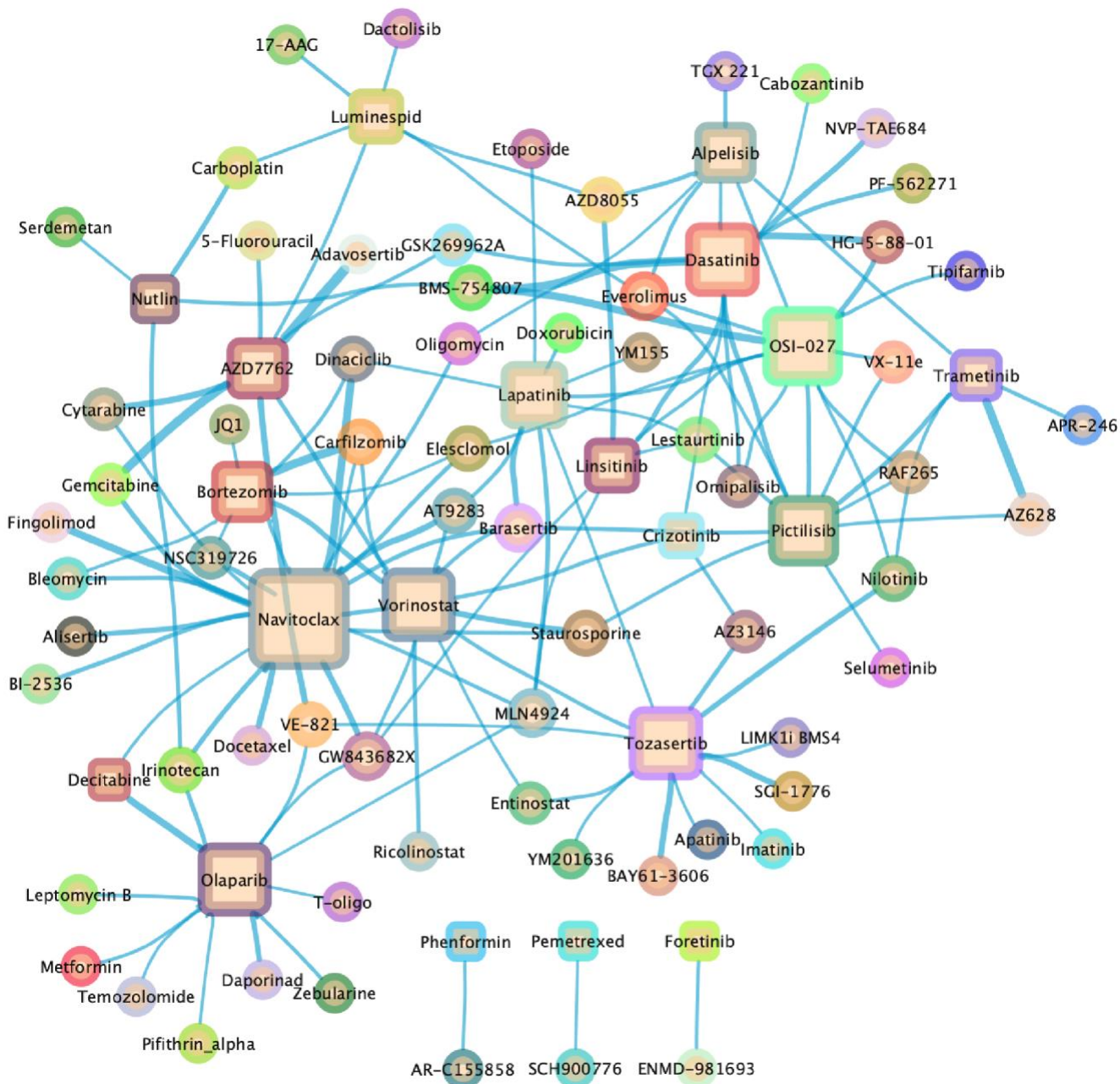


B



**Supplementary Figure 7: Aurora kinase inhibitors are engaged more frequently in synergistic and HSA events than CDK inhibitors. A, Pattern of synergy and HSA events across**

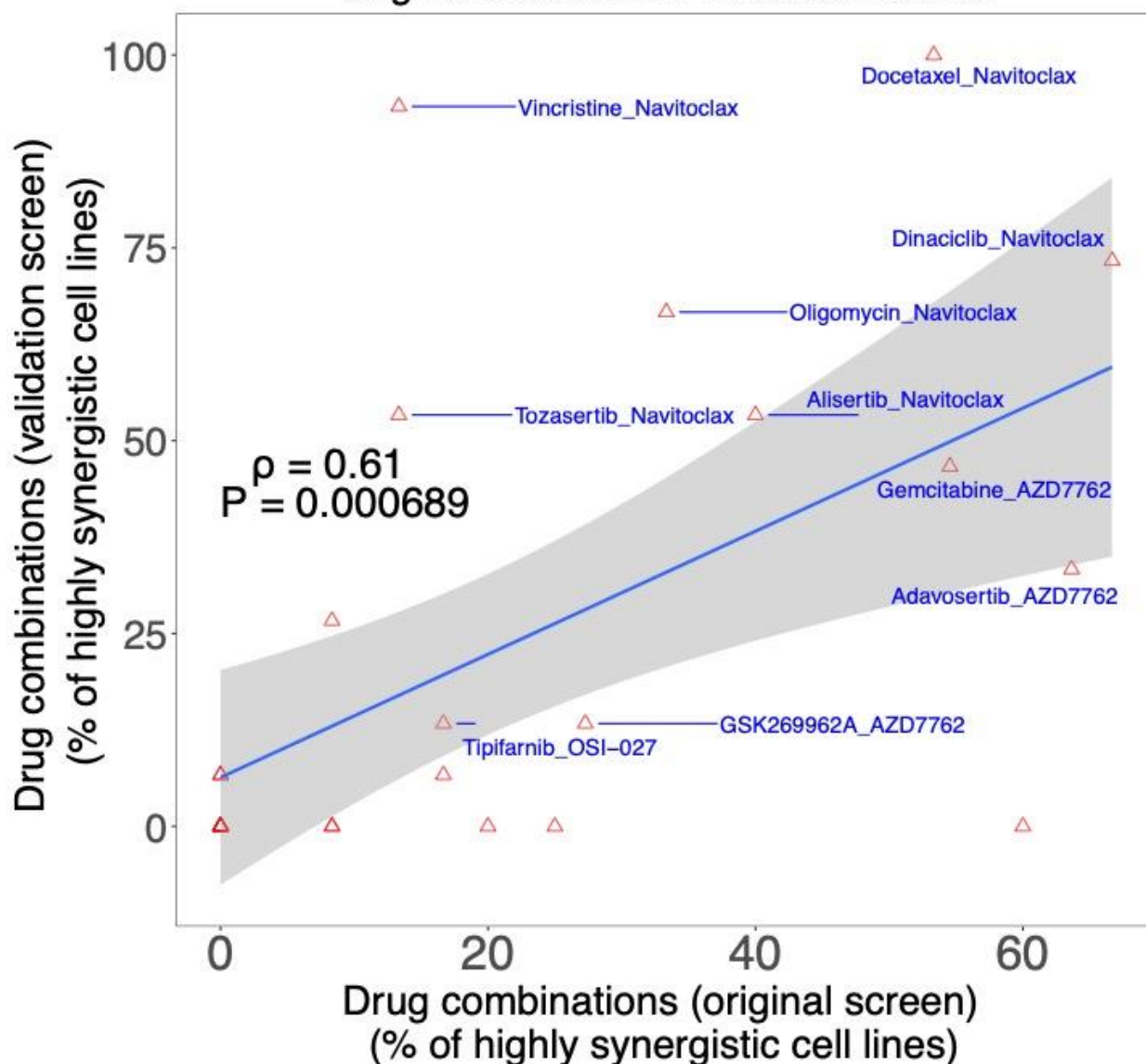
selected anchors for the library drugs targeting Aurora Kinases and CDKs. B, Impact score graphs for Aurora Kinase and CDK inhibitors.



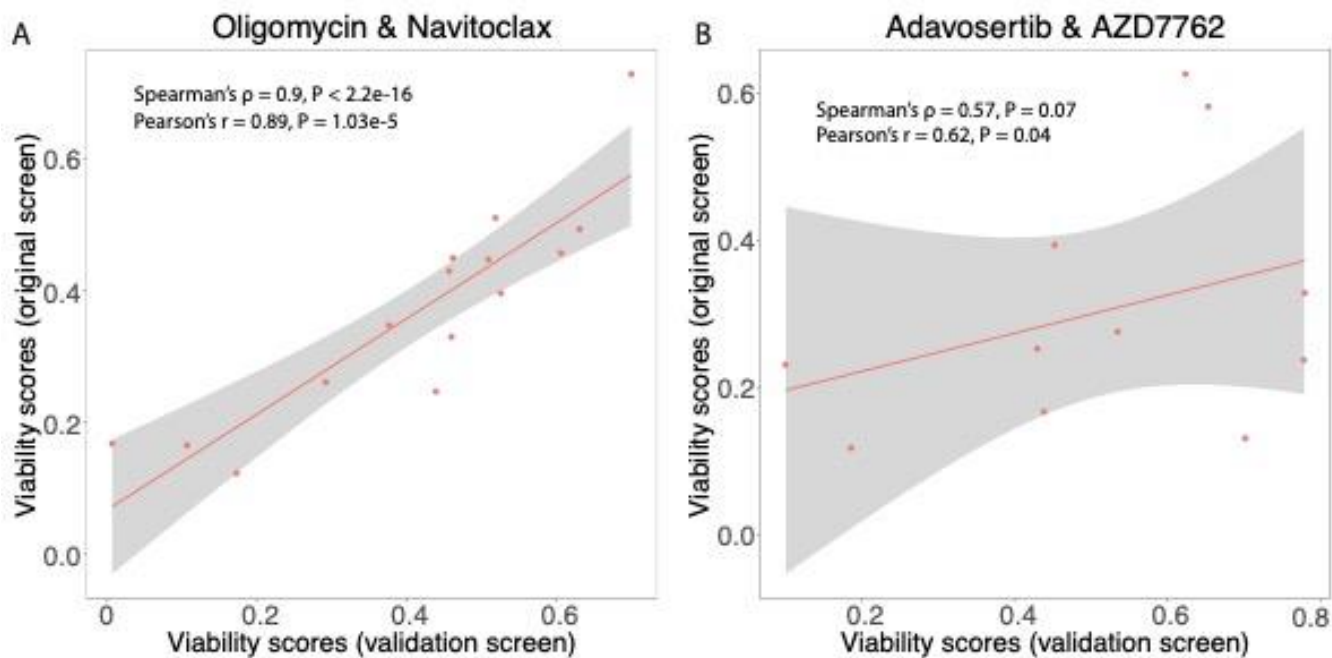
**Supplementary Figure 8: Network representation of drug-drug interactions for top 5% synergistic events across all drugs and anchors.** Anchor drugs are represented as squares and library drugs as circles. The size of the anchor nodes is proportional to the number of synergistic

events the corresponding drug is involved in. The thickness of the edge between two drugs corresponds to the median value of the synergy scores across all cell lines.

### Correlation of high synergies between original screen and validation screen

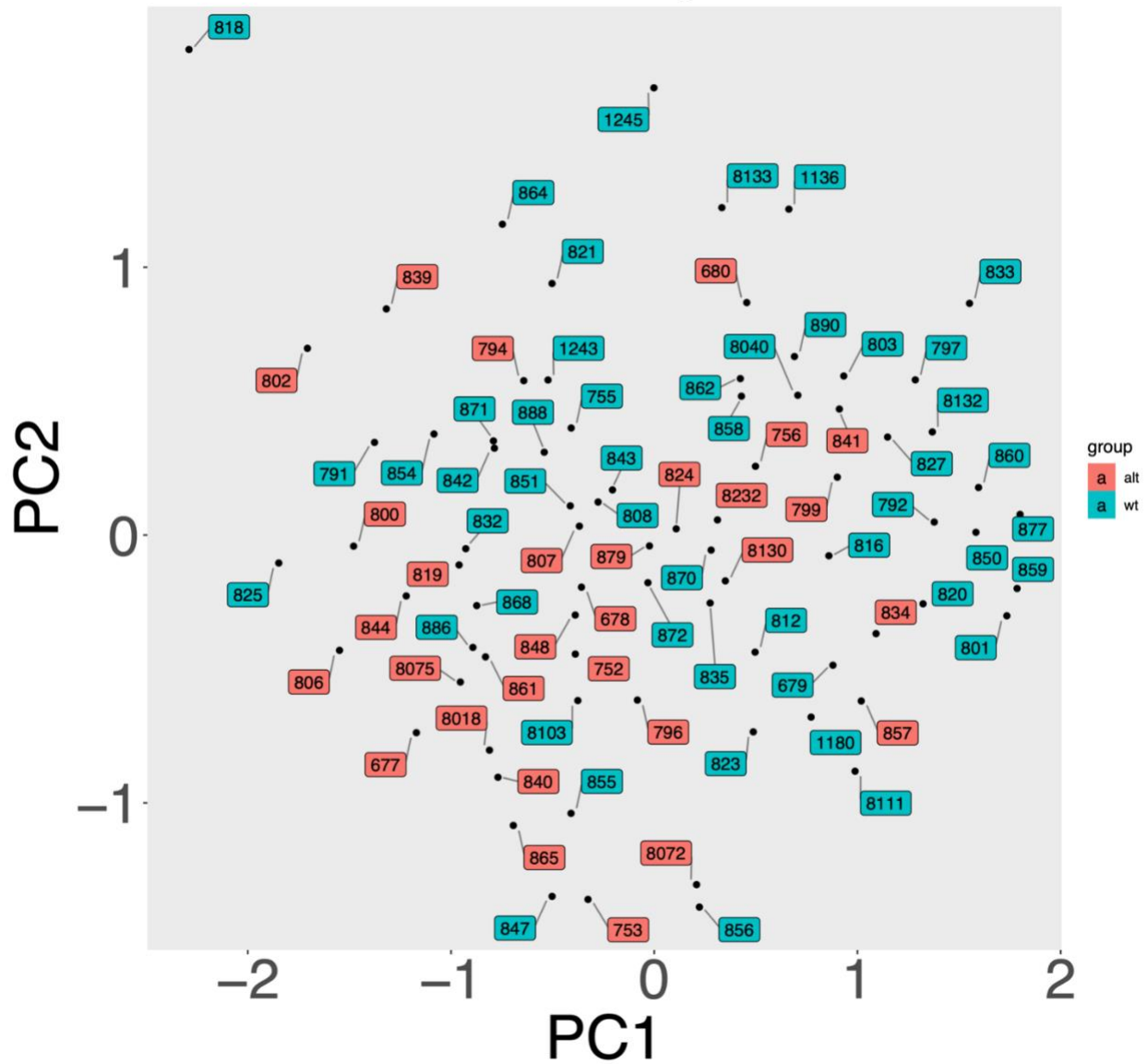


**Supplementary figure 9: Validation of high synergistic drug combinations between the original and validation screens.** Each drug combination is ranked based on the percentage of cell lines in which they are highly synergistic (Methods), in the original and in the validation screens. Spearman's correlation and p-value between the rankings of the drug combinations between the original and validation screens are shown. Overall, 27 common drug combinations were tested in both screens. Only some drug combination names are displayed for the sake of clarity.



**Supplementary figure 10: Correlation between the viability scores of two drug combinations between the original screen and validation screen across all 15 NSCLC cell lines.** (A) Oligomycin and Navitoclax; (b) Adavosertib and AZD7762. The correlation values for all 29 drug combinations are shown in Supp. Data S10A. Spearman and Pearson correlations and p-values are shown. When P was reported as 0 by the software, it is written as  $P < 2.2e-16$ .

# Cell line similarity -- KRAS



**Supplementary Figure 11: Analysis of synergy patterns across drugs for each cell line does not differentiate KRAS WT from KRAS mutant cell lines.** Principle component analysis was used to analyze the proximity of cell lines based on the pattern of synergistic events across all anchors and library drugs. Cell lines are color coded based on KRAS mutational status.



## Supplementary References

- 1 Goldoni, M. & Johansson, C. A mathematical approach to study combined effects of toxicants in vitro: evaluation of the Bliss independence criterion and the Loewe additivity model. *Toxicol In Vitro* **21**, 759-769 (2007). <https://doi.org:10.1016/j.tiv.2007.03.003>
- 2 Chandu, D. P. Improved greedy algorithm for set covering problem. *arXiv preprint arXiv:1506.04220* (2015).
- 3 Chvatal, V. A greedy heuristic for the set-covering problem. *Mathematics of operations research* **4**, 233-235 (1979).
- 4 Grossman, T., ; Wool, A. . Computational experience with approximation algorithms for the set covering problem. *European journal of operational research* **101**, 81-92 (1997).
- 5 Bajrami, I. *et al.* Synthetic lethality of PARP and NAMPT inhibition in triple-negative breast cancer cells. *EMBO Mol Med* **4**, 1087-1096 (2012). <https://doi.org:10.1002/emmm.201201250>
- 6 Heske, C. M. *et al.* Matrix Screen Identifies Synergistic Combination of PARP Inhibitors and Nicotinamide Phosphoribosyltransferase (NAMPT) Inhibitors in Ewing Sarcoma. *Clin Cancer Res* **23**, 7301-7311 (2017). <https://doi.org:10.1158/1078-0432.CCR-17-1121>
- 7 Harrington, L. S., Findlay, G. M. & Lamb, R. F. Restraining PI3K: mTOR signalling goes back to the membrane. *Trends Biochem Sci* **30**, 35-42 (2005). <https://doi.org:10.1016/j.tibs.2004.11.003>
- 8 Yoneyama, Y. *et al.* Serine Phosphorylation by mTORC1 Promotes IRS-1 Degradation through SCFbeta-TRCP E3 Ubiquitin Ligase. *iScience* **5**, 1-18 (2018). <https://doi.org:10.1016/j.isci.2018.06.006>
- 9 Kovalski, J. R., Shanderson, R. L. & Khavari, P. A. Ras functional proximity proteomics establishes mTORC2 as new direct ras effector. *Oncotarget* **10**, 5126-5135 (2019). <https://doi.org:10.18632/oncotarget.27025>
- 10 Asghar, U., Witkiewicz, A. K., Turner, N. C. & Knudsen, E. S. The history and future of targeting cyclin-dependent kinases in cancer therapy. *Nat Rev Drug Discov* **14**, 130-146 (2015). <https://doi.org:10.1038/nrd4504>
- 11 Fry, D. W. *et al.* Specific inhibition of cyclin-dependent kinase 4/6 by PD 0332991 and associated antitumor activity in human tumor xenografts. *Mol Cancer Ther* **3**, 1427-1438 (2004).
- 12 Cristofanilli, M. *et al.* Fulvestrant plus palbociclib versus fulvestrant plus placebo for treatment of hormone-receptor-positive, HER2-negative metastatic breast cancer that progressed on previous endocrine therapy (PALOMA-3): final analysis of the multicentre, double-blind, phase 3 randomised controlled trial. *Lancet Oncol* **17**, 425-439 (2016). [https://doi.org:10.1016/S1470-2045\(15\)00613-0](https://doi.org:10.1016/S1470-2045(15)00613-0)
- 13 Lim, J. S., Turner, N. C. & Yap, T. A. CDK4/6 Inhibitors: Promising Opportunities beyond Breast Cancer. *Cancer Discov* **6**, 697-699 (2016). <https://doi.org:10.1158/2159-8290.CD-16-0563>
- 14 Puyol, M. *et al.* A synthetic lethal interaction between K-Ras oncogenes and Cdk4 unveils a therapeutic strategy for non-small cell lung carcinoma. *Cancer Cell* **18**, 63-73 (2010). <https://doi.org:10.1016/j.ccr.2010.05.025>

- 15 Patnaik, A. *et al.* Efficacy and Safety of Abemaciclib, an Inhibitor of CDK4 and CDK6, for Patients with Breast Cancer, Non-Small Cell Lung Cancer, and Other Solid Tumors. *Cancer Discov* **6**, 740-753 (2016). <https://doi.org:10.1158/2159-8290.CD-16-0095>
- 16 Pacheco, J. & Schenk, E. CDK4/6 inhibition alone and in combination for non-small cell lung cancer. *Oncotarget* **10**, 618-619 (2019). <https://doi.org:10.18632/oncotarget.26545>
- 17 Xue, Y. *et al.* SMARCA4 loss is synthetic lethal with CDK4/6 inhibition in non-small cell lung cancer. *Nat Commun* **10**, 557 (2019). <https://doi.org:10.1038/s41467-019-08380-1>
- 18 Wander, S. A. *et al.* The Genomic Landscape of Intrinsic and Acquired Resistance to Cyclin-Dependent Kinase 4/6 Inhibitors in Patients with Hormone Receptor-Positive Metastatic Breast Cancer. *Cancer Discov* **10**, 1174-1193 (2020). <https://doi.org:10.1158/2159-8290.CD-19-1390>
- 19 Hafner, M. *et al.* Multiomics Profiling Establishes the Polypharmacology of FDA-Approved CDK4/6 Inhibitors and the Potential for Differential Clinical Activity. *Cell Chem Biol* **26**, 1067-1080 e1068 (2019). <https://doi.org:10.1016/j.chembiol.2019.05.005>
- 20 Thomas, S. M. & Brugge, J. S. Cellular functions regulated by Src family kinases. *Annu Rev Cell Dev Biol* **13**, 513-609 (1997). <https://doi.org:10.1146/annurev.cellbio.13.1.513>
- 21 Begley, M. J. *et al.* EGF-receptor specificity for phosphotyrosine-primed substrates provides signal integration with Src. *Nat Struct Mol Biol* **22**, 983-990 (2015). <https://doi.org:10.1038/nsmb.3117>
- 22 Jabbour, E. & Kantarjian, H. Chronic myeloid leukemia: 2020 update on diagnosis, therapy and monitoring. *Am J Hematol* **95**, 691-709 (2020). <https://doi.org:10.1002/ajh.25792>
- 23 Galkin, A. V. *et al.* Identification of NVP-TAE684, a potent, selective, and efficacious inhibitor of NPM-ALK. *Proc Natl Acad Sci U S A* **104**, 270-275 (2007). <https://doi.org:10.1073/pnas.0609412103>
- 24 Seashore-Ludlow, B. *et al.* Harnessing Connectivity in a Large-Scale Small-Molecule Sensitivity Dataset. *Cancer Discov* **5**, 1210-1223 (2015). <https://doi.org:10.1158/2159-8290.CD-15-0235>
- 25 Zullo, K. M. *et al.* Aurora A Kinase Inhibition Selectively Synergizes with Histone Deacetylase Inhibitor through Cytokinesis Failure in T-cell Lymphoma. *Clin Cancer Res* **21**, 4097-4109 (2015). <https://doi.org:10.1158/1078-0432.CCR-15-0033>
- 26 Bertolin, G. *et al.* Aurora kinase A localises to mitochondria to control organelle dynamics and energy production. *Elife* **7** (2018). <https://doi.org:10.7554/eLife.38111>
- 27 Bertolin, G. & Tramier, M. Insights into the non-mitotic functions of Aurora kinase A: more than just cell division. *Cell Mol Life Sci* **77**, 1031-1047 (2020). <https://doi.org:10.1007/s00018-019-03310-2>
- 28 Otto, T. *et al.* Stabilization of N-Myc is a critical function of Aurora A in human neuroblastoma. *Cancer Cell* **15**, 67-78 (2009). <https://doi.org:10.1016/j.ccr.2008.12.005>
- 29 Crystal, A. S. *et al.* Patient-derived models of acquired resistance can identify effective drug combinations for cancer. *Science* **346**, 1480-1486 (2014). <https://doi.org:10.1126/science.1254721>
- 30 Donnelly, H. J. *et al.* Kinome rewiring reveals AURKA limits PI3K-pathway inhibitor efficacy in breast cancer. *Nat Chem Biol* **14**, 768-777 (2018). <https://doi.org:10.1038/s41589-018-0081-9>

- 31 Shah, K. N. *et al.* Aurora kinase A drives the evolution of resistance to third-generation EGFR inhibitors in lung cancer. *Nat Med* **25**, 111-118 (2019).  
<https://doi.org:10.1038/s41591-018-0264-7>
- 32 Friedman, A. A. *et al.* Landscape of Targeted Anti-Cancer Drug Synergies in Melanoma Identifies a Novel BRAF-VEGFR/PDGFR Combination Treatment. *Plos One* **10**, e0140310 (2015). <https://doi.org:10.1371/journal.pone.0140310>
- 33 Guieze, R. *et al.* Mitochondrial Reprogramming Underlies Resistance to BCL-2 Inhibition in Lymphoid Malignancies. *Cancer Cell* **36**, 369-384 e313 (2019).  
<https://doi.org:10.1016/j.ccell.2019.08.005>
- 34 Gross, A. & Katz, S. G. Non-apoptotic functions of BCL-2 family proteins. *Cell Death Differ* **24**, 1348-1358 (2017). <https://doi.org:10.1038/cdd.2017.22>
- 35 Gao, H. *et al.* High-throughput screening using patient-derived tumor xenografts to predict clinical trial drug response. *Nat Med* **21**, 1318-1325 (2015).  
<https://doi.org:10.1038/nm.3954>